Med Biol Eng Comput (2013) 51:1235–1250
DOI 10.1007/s11517-013-1044-7

SPECIAL ISSUE - REVIEW

Understanding the mechanisms amenable to CRT response: from pre-operative multimodal image data to patient-specific computational models

C. Tobon-Gomez · N. Duchateau · R. Sebastian · S. Marchesseau · O. Camara · E. Donal · M. De Craene · A. Pashaei · J. Relan · M. Steghofer · P. Lamata · H. Delingette · S. Duckett · M. Garreau · A. Hernandez · K. S. Rhode · M. Sermesant · N. Ayache · C. Leclercq · R. Razavi · N. P. Smith · A. F. Frangi

Received: 24 April 2012 / Accepted: 2 February 2013 / Published online: 21 February 2013
© International Federation for Medical and Biological Engineering 2013

Abstract This manuscript describes our recent developments towards better understanding of the mechanisms amenable to cardiac resynchronization therapy response. We report the results from a full multimodal dataset corresponding to eight patients from the euHeart project. The datasets include echocardiography, MRI and electrophysiological studies. We investigate two aspects. The first one focuses on pre-operative multimodal image data. From 2D echocardiography and 3D tagged MRI images, we compute atlas based *dyssynchrony indices*. We complement these indices with presence and extent of scar tissue and correlate them with CRT response. The second one focuses on computational models. We use pre-operative imaging to generate a patient-specific computational model. We show results of a fully automatic personalized electromechanical simulation. By case-per-case discussion of the results, we highlight the potential and key issues of this multimodal pipeline for the understanding of the mechanisms of CRT response and a better patient selection.

Keywords Cardiac resynchronization therapy · Dyssynchrony indices · Computational models · Patient-specific simulation

Electronic supplementary material The online version of this article (doi:10.1007/s11517-013-1044-7) contains supplementary material, which is available to authorized users.

C. Tobon-Gomez (✉) · N. Duchateau · O. Camara · M. De Craene · A. Pashaei · M. Steghofer · A. F. Frangi
CISTIB, Universitat Pompeu Fabra, Barcelona, Spain
e-mail: catactg@gmail.com

C. Tobon-Gomez · N. Duchateau · O. Camara · M. De Craene · A. Pashaei · M. Steghofer · A. F. Frangi
CIBER-BBN, Barcelona, Spain

C. Tobon-Gomez · O. Camara
PhySense, Universitat Pompeu Fabra, Barcelona, Spain

N. Duchateau
Hospital Clínic, Institut d'Investigacions Biomèdiques August Pi i Sunyer, Universitat de Barcelona, Barcelona, Spain

R. Sebastian
Computational Multi-Scale Physiology Lab, Universitat de Valencia, Valencia, Spain

S. Marchesseau · J. Relan · H. Delingette · M. Sermesant · N. Ayache
INRIA Méditerranée, Asclepios Project, Sophia Antipolis, France

E. Donal · M. Garreau · A. Hernandez · C. Leclercq
INSERM, U1099, 35000 Rennes, France

E. Donal · M. Garreau · A. Hernandez · C. Leclercq
Université de Rennes 1, LTSI, 35000 Rennes, France

E. Donal · C. Leclercq
CHU Rennes, Service de Cardiologie et Maladies Vasculaires, 35000 Rennes, France

M. De Craene
Philips Research, Medisys, Suresnes, France

P. Lamata · N. P. Smith
Department of Computer Science, University of Oxford, Oxford, UK

P. Lamata · S. Duckett · K. S. Rhode · R. Razavi · N. P. Smith
Division of Imaging Sciences and Biomedical Engineering, King's College London, London, UK

A. F. Frangi
Department of Mechanical Engineering, University of Sheffield, Sheffield, UK

1 Introduction

Cardiac resynchronization therapy (CRT) can relieve heart failure (HF) symptoms by reducing heart dyssynchrony through the implantation of a pacemaker. However, non-response rates to CRT rise to 30 % (clinical response) or 44 % (volume response) [5]. Thus, patient selection and pacemaker configurations remain open challenges of high concern and focus within the clinical community. Recent updates of the official guidelines for CRT from the European Society of Cardiology now include a number of additional patient subgroups that were previously omitted [32]. Several research groups are also investigating new pacing configurations (number and position of leads) in experimental models under fully controlled conditions [47] as well as the different parameters that are related to response to CRT [4].

Patient-specific cardiac imaging tools and computational models can help to understand and improve CRT, since they combine anatomical and functional pre-operative data to provide new insights into dyssynchrony mechanics [41]. This has motivated our research under two driving questions: (1) Can pre-operative multimodal image data improve our understanding of the mechanisms of CRT response? (2) Can in silico electromechanical simulations improve our understanding of intra-ventricular mechanical dyssynchrony? This manuscript describes our recent developments towards answering these two questions. These developments have been applied to clinical cases collected for a multi-center study within the euHeart project. Most of the components presented in this work are already integrated into a common software framework, constituting the *cardiac resynchronization therapy planning platform*, currently implemented in an open-source software, GIMIAS [26].

2 Image data

The image data collected routinely before CRT implantation is mainly echocardiography, for cost and practical reasons. Next to a full echocardiographic evaluation, often patients undergo an MRI scan to evaluate the presence and extent of scar tissue in the myocardium. Follow-up with MRI is currently not feasible for implanted patients. With this starting point, we have extended each examination to include advanced acquisition sequences to better understand the mechanisms of dyssynchrony and relate them to CRT response.

2.1 Patient description

In this study, we report the results obtained in a full dataset of multimodal data corresponding to eight patients: four acquired at INSERM (Institut National de la Santé et de la Recherche Médicale, Université de Rennes, France), and four acquired at KCL (King's College London, UK). These patients are a subset of a larger multi-center study ($n = 70$) within the euHeart project. These cases were selected to high-light different aspects of our pipeline. All patients were selected for CRT implantation based on standard criteria [New York Heart Association (NYHA) class III–IV; left Ventricular (LV) end-diastolic diameter >55 mm; LV

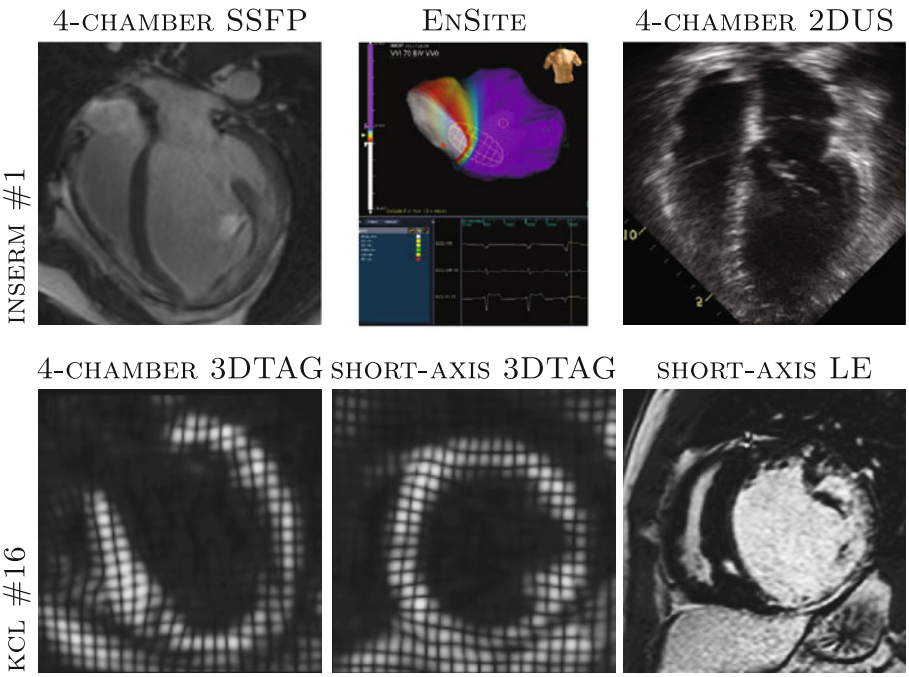

Fig. 1 Image data of patient INSERM #1 (*top*): pre-CRT MRI (4-chamber SSFP), intra-operative electrophysiological study (EnSite), displaying a voltage map at the end of the QRS complex, follow-up echocardiography (4-chamber 2DUS). Image data of patient KCL #16 (*bottom*): pre-CRT 3DTAG in 4-chamber and short-axis view, pre-CRT LE in short-axis view

Table 1 Patient demographics evaluated at pre- (basal) and post-CRT (follow-up)

	INSERM				KCL			
	#1	#2	#3	#4	#12	#9	#16	#24
Demographics								
Age	46	72	69	51	70	72	32	56
Ischemic etiology	No	No	No	No	Yes	Yes	Yes	No
QRS width (ms)								
Basal	190	156	139	170	160	160	135	160
Follow-up	154	147	152	122	200	120	–	160
6MWT (m)								
Basal	522	360	441	423	220	210	350	390
Follow-up	534	456	436	486	390	430	445	–
NYHA								
Basal	III	III	III	III	III	III	III	III
Follow-up	II	II	II	II	I	I	II	I
LV ED diameter (mm)								
Basal	72	64	64	78	59	58	78	76
Follow-up	56	63	64	65	–	66	–	72
LV EDV (ml)								
Basal	376[a]	327[a]	190[a]	274	142	243	385	250
Follow-up	150	216	140	160	177	222	367	235
LV ESV (ml)								
Basal	277[a]	249[a]	123[a]	223	92	184	319	213
Follow-up	93	126	86	104	116	172	272	171
LV EF (%)								
Basal	26	24	35	19	35	24	17	15
Follow-up	38	42	39	35	34	23	26	27
Infarct (LE)								
Location	N	N	N	N	Sep	Sep	Inf	N
Clinical response								
Increase in 6MWT (%)	2	27	−1	15	77	105	27	–
Reduction in NYHA	1	1	1	1	2	2	1	2
Patient/healthy 6MWT (%)[b]								
Basal	91	63	77	74	39	37	61	68
Follow-up	94	80	76	85	68	75	78	–
Volume response								
ESV reduction (%)	–	–	–	53	– 26	7	15	20
Increase in EF (%)	44	75	11	88	–2	–7	51	84
Spectrum of responses[c]								
Pure LBBB with SF	R	–	–	R	–	–	–	R
LBBB with sep scar	–	–	–	–	NR	NR	–	–
LBBB with non-sep scar	–	–	–	–	–	–	R	–
Other mechanisms	–	R	NR	–	–	–	–	–

6MWT 6-min walking test, *EDV* end diastolic volume, *ESV* end systolic volume, *EF* ejection fraction, *LE* late enhancement, *N* none, *Sep* septal, *Inf* inferior, *LBBB* left bundle branch block, *SF* septal flash, *R* responder, *NR* non-responder

[a] Measurement from MRI

[b] 57 m [8]

[c] See Sect. 5.1

ejection fraction (EF) <35 % and prolonged QRS on electrocardiogram >120 ms]. The study complied with the Declaration of Helsinki and the protocol was accepted by our local ethics committees. Written informed consent was obtained from all subjects. Patient demographics are shown in Table 1.

To evaluate patient response to CRT, there are usually two main criteria: *clinical response* and *volume response*. In this paper, we defined clinical response as an increase ≥10 % in the 6-min walking test (6MWT), or a NYHA functional class reduction ≥1 point for patients unable to complete the 6-min walking test at baseline. Volume response is defined as a reduction ≥15% in LV end-systolic volume or an increase ≥15% in ejection fraction [5]. These criteria (evaluated in Table 1) are in agreement with clinical practice and values found in literature. For limitations of using strict cut-off values refer to Sect. 5.1.

2.2 Ultrasound acquisition

Patients underwent a full echocardiographic study (2DUS) prior to CRT intervention and at 3/6 months follow-up. The studies were acquired using a GE Vivid 7 scanner (GE Healthcare, Milwaukee, WI, US). Ejection fraction (EF) and LV dimension were measured for each patient using 2D biplane Simpson's method. Analysis was performed using the EchoPac software (General Electric-Vingmed, Milwaukee, WI, US). For an example dataset see Fig. 1.

2.3 MRI acquisition

The MR datasets were acquired using a 1.5T Philips Achieva System (Philips Healthcare, Best, The Netherlands). The MR sequences used in this study were cine steady-state free precession (SSFP), late enhancement (LE) and 3D tagged (3DTAG) images. SSFP datasets were scanned in multiple views (Repetition Time/Echo Time 2.9/1.5 ms, flip angle 40°). For an example dataset see

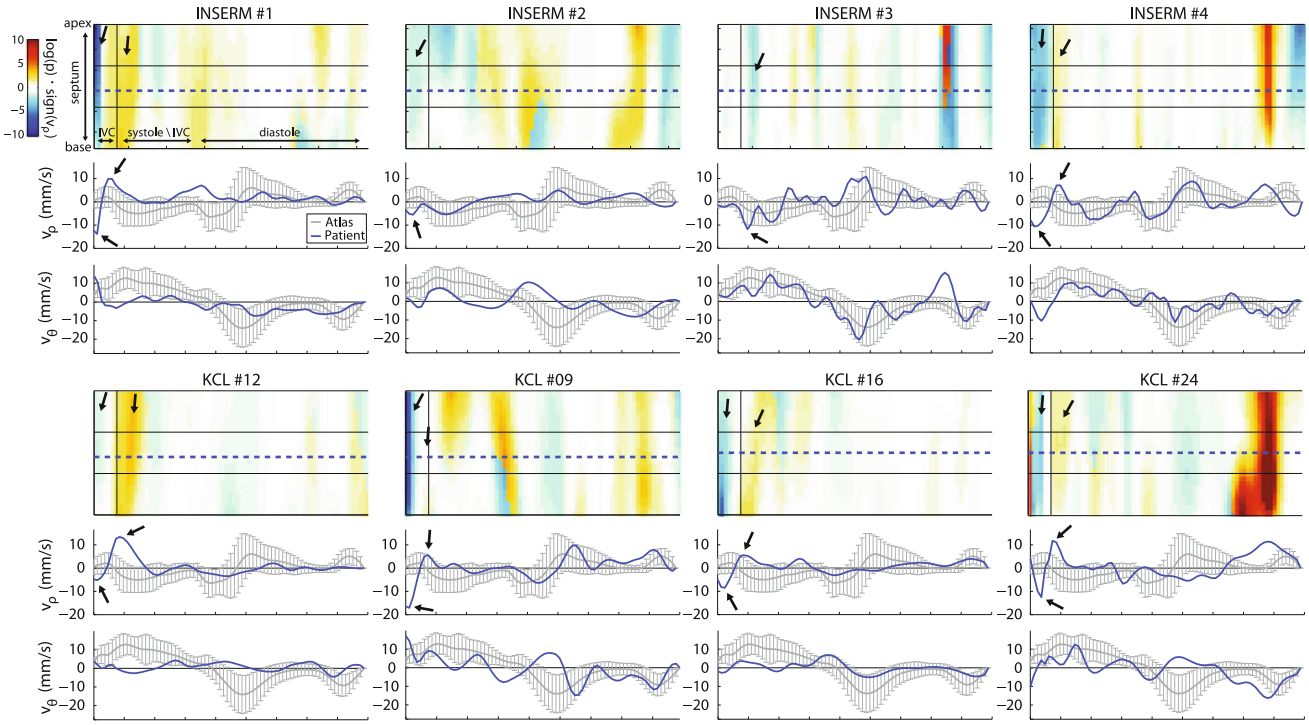

Fig. 2 2D+t motion abnormality quantification. The atlas-based dyssynchrony indices are represented by means of *color-coded maps*, in which the horizontal axis is time (one cardiac cycle) and the vertical one is the position along the septum. Since the velocity data has been aligned to a common spatiotemporal system of coordinates, the time axis is the same for all subjects (axis legends are given for subject INSERM #1 only, for the sake of clarity). Values correspond to the p value index used to locally encode abnormality, in a logarithmic scale, multiplied by the sign of the radial velocity. Thus, *blue* and *red colors* indicate highly abnormal inward and outward motion of the septum, respectively, while *white color* corresponds to normal motion. The *vertical line* indicates the end of the isovolumetric contraction (IVC) period. The presence of inward and outward events are indicated by the *black arrows* (see animations in supplementary material). The dyssynchrony patterns inward/outward with no longitudinal velocity (KCL #12) and inward only (KCL #9) are probably due to the presence of septal scar (see Fig. 3). $\mathbf{v}_\rho$ = radial velocity, $\mathbf{v}_\theta$ = longitudinal velocity (color figure online)

Fig. 1. LE images were also scanned in multiple views with an inversion recovery sequence, 10 min after IV administration of 0.2 mmol/kg of gadopentate dimeglumine contrast (Repetition Time/Echo Time 5.7/1.9 ms, flip angle 25°). 3DTAG datasets were obtained with three sequential breath-hold acquisitions in each orthogonal direction (Repetition Time/Echo Time 7.0/3.2 ms, flip angle 19°–25°, tag distance 7 mm) [39]. A respiratory navigator was used to compensate for possible respiratory miss-alignment during the three sequential acquisitions.

2.4 Electrophysiological study acquisition

Cardiac electrophysiological studies were performed for INSERM patients, using the EnSite Velocity system (St Jude Medical, St Paul, MN, US). For an example see Fig. 1. A 64-electrode balloon catheter was inserted through the femoral artery and placed within the left ventricle. Recordings were obtained while performing different stimulation configurations with the implanted CRT system. Raw far-field potentials acquired by each electrode, as well as a set of virtual electrograms projected onto the endocardial surface, were exported for further processing, which involved the estimation of local endocardial activation times (LAT) and the generation of isochronal and isopotential maps [37].

3 Can pre-operative multimodal image data improve our understanding of the mechanisms of CRT response?

The limitations of single measurements of mechanical dyssynchrony have been extensively discussed [23], and recent works insist on the importance of understanding the complexity and variety of the etiologies of cardiac dyssynchrony [27, 34]. Keeping this in mind, we chose to analyze pre-operative image data in a way that allows both the characterization and quantification of septal deformation patterns (i.e., septal flash[1]). Doing this we compute a

[1] Early inward motion/contraction of the septum, followed by lateral wall contraction. This latter contraction pulls the relaxed septum and thereby *stretches* it (see animations in supplementary material).

dyssynchrony index at each spatiotemporal location, which consists of a distance to normality in terms of motion. In this work, we computed such dyssynchrony indices from the CRT pre-operative datasets we collected, namely 2DUS images (Sect. 3.1) and 3DTAG MR images (Sect. 3.2).

3.1 2D+t motion abnormality quantification

A new methodology for the computation of *atlas-based* dyssynchrony indices was implemented in [17]. The methodology was tested on 88 CRT candidates with visual evidence of abnormal septal motion [18]. Briefly, this method compares the myocardial motion pattern of the studied subject to an atlas of normal motion built from a population of healthy volunteers (in the present study, 21 healthy volunteers with normal cardiac function recruited at the Hospital Clínic, Barcelona, Spain). This method consists of three steps.

3.1.1 Myocardial velocities

Extraction of myocardial motion (myocardial velocities), which is achieved in this study through the temporal diffeomorphic free form deformation (TDFFD) registration algorithm [13, 14]. The TDFFD approach enforces the temporal consistency and differentiability of the recovered 2D+t velocities, which should be preferred for the atlas building process [16].

3.1.2 Alignment

Spatiotemporal alignment to a common reference anatomy, using the matching of physiological events (time) and FFD image registration (space).

3.1.3 Statistics

Computation of statistics to encode normal motion within the healthy population (average and covariance), and to quantify abnormality (p value resulting from the Mahalanobis distance being used as statistical distance to normality, low p value meaning high degree of abnormality).

For 2D+t data, these indices are represented by means of color-coded maps, in which the septum has been unfolded around its medial line and used as vertical dimension, time being used as horizontal axis (Fig. 2). Blue color represents highly abnormal inward motion of the septum, whereas red color represents highly abnormal outward motion. No abnormality is, therefore, represented by white color.

3.2 3D+t motion abnormality quantification

To extend the quantification of dyssynchrony indices to 3D+t data, we collected a database of 15 volunteers to have a reference of normal motion [44]. The volunteers were scanned at KCL following the protocol described in Sect. 2. Motion was quantified using the TDFFD algorithm, which has been tested on 3DUS datasets [14] and 3DTAG MRI datasets [15]. In our case, we used the 3DTAG datasets to compute the atlas of myocardial velocities. Briefly, due to our TDFFD approach, motion (myocardial velocities) is represented by a 3D+t diffeomorphic transformation continuous in space and time. Abnormal motion is quantified using statistical parametric mapping (SPM) [49] analysis on the velocity fields. Similarly to our 2D+t approach, SPM provides a map of p values, which grades and localizes regions where the two populations under comparison differ significantly (individual vs. volunteer). Dyssynchrony is associated with a simultaneous event of contraction and relaxation. Such an event triggers high abnormality values (i.e., high p value of ϵ). They are noticeable in Fig. 4 as peaks in the plot and yellow areas on the left ventricular surfaces. The plots were computed averaging the AHA segments along the septal wall at basal and midventricular level. Further details can be found in [12].

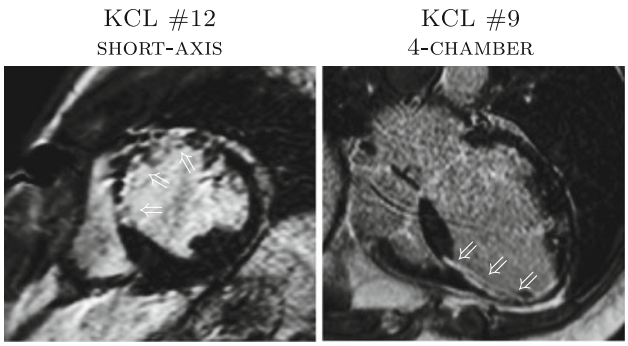

Fig. 3 Late enhancement images highlighting the presence of septal scar (*white arrows*). This is most likely the reason for the dyssynchrony patterns displayed by these two patients

3.3 Resulting dyssynchrony indices

This section presents the results obtained from 2D and 3D dyssynchrony indices. These results are further discussed in Sect. 5.

3.4 INSERM patients

3.4.1 Prediction

Based on the abnormality maps (Fig. 2), patients #1 and #4 presented septal flash (SF) with no other complications and were expected to be responders, following the results of Parsai et. al. [34]. Patient #2 presented passive motion on the septum (inward motion during early systole, not followed by outward during early isovolumetric contraction).

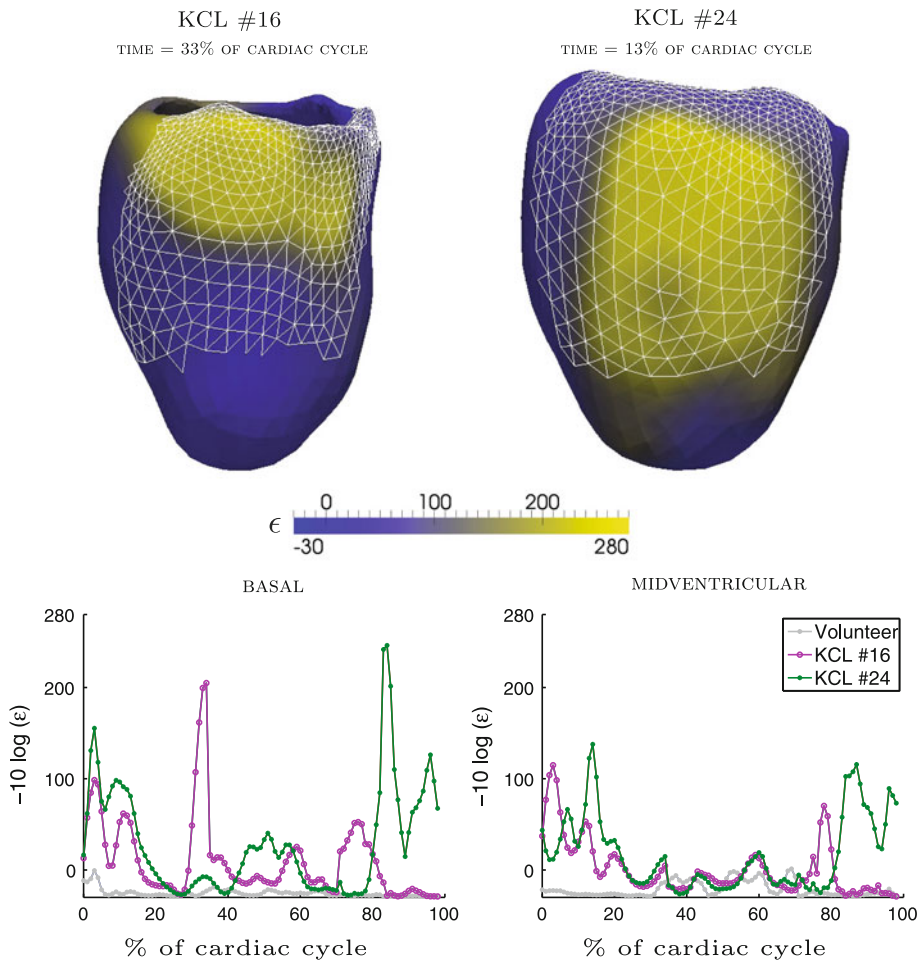

Fig. 4 3D+t motion abnormality quantification computed from 3DTAG datasets. *p* value associated to the Euler characteristic was plotted as a *color map* (*top*) and as a function of time (*bottom*). Abnormal motion results in high values of ϵ and are visualized as peaks in the plot and *yellow areas* in the *color map*. The plots were computed averaging the AHA segments along the septal wall at basal and midventricular level. The *white wireframe* represents the AHA segments used to calculate the plots (color figure online)

In this case was hard to predict CRT response. The 2DUS images of patient #3 were of relatively bad quality. However, we could differentiate almost normal longitudinal contraction and small abnormal radial motion of the septum.

3.4.2 Response

Considering the information in Table 1, and based on volume response, patients #1, #2 and #4 were clear responders to CRT. On the other hand, patient #3 was a non-responder. The patient maintains a large QRS width, probably indicating that electrical dyssynchrony (not LBBB in this case) was not corrected. This patient has different etiology than the other cases (idiopathic cardiomyopathy), along with mitral and aortic regurgitation, significant atrial volumes and increased pulmonary artery pressure. This condition makes the evaluation of CRT response more difficult. For these 3 volume responders, patient #1 did not meet the clinical response criteria. However, the distance walked by this patient at baseline was very close to normal (91 % compared to a healthy population 40–80 years old) [8]. Therefore, 6WMT distance is probably a suboptimal criterium for this case. These results are further discussed in Sect. 5.

3.5 KCL patients

3.5.1 Prediction

Based on the abnormality maps (Fig. 2), patient #12 presented inward–outward motion, but no longitudinal motion. Patient #9 presented inward motion only. This correlates with the presence of scar along the septal wall (Fig. 3), in accordance with other clinical studies [20]. Patient #16 presented SF, more marked at basal level, and end-systole outward motion. The scar of this patient was located at inferior wall. Patient #24 showed large SF along the whole septum.

We also computed dyssynchrony indices from 3DTAG images for patients KCL #16 and KCL #24. Both patients displayed abnormal motion at early systole and at late diastole. The early systole (33 % of cardiac cycle) abnormality motion of patient KCL #16 is mainly localized at basal level (consistent with 2DUS observations). The early systole (13 % of cardiac cycle) abnormality motion of

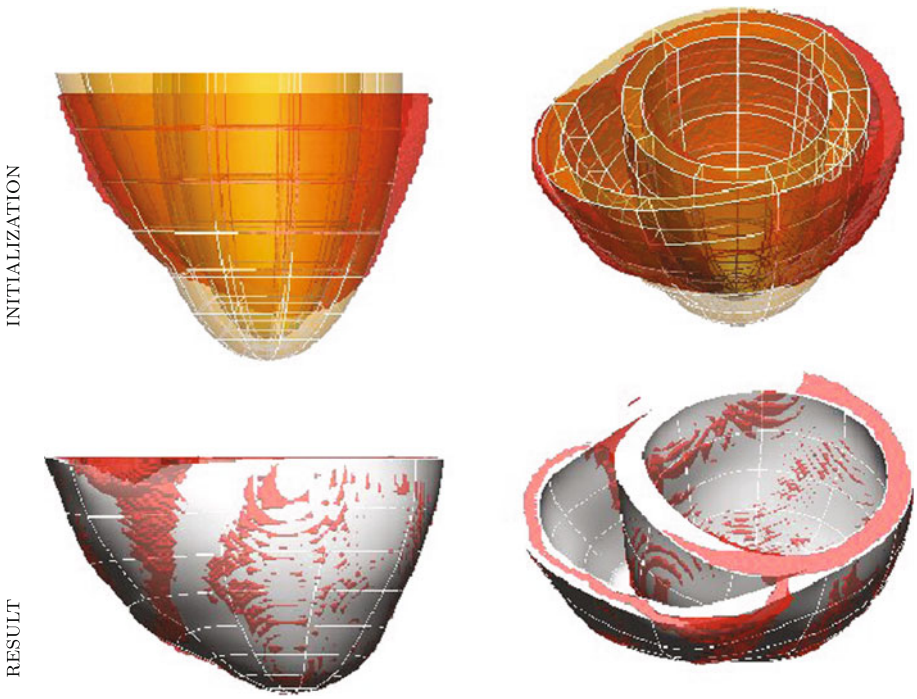

Fig. 5 Personalized cubic Hermite mesh: template mesh initialization (*top*) and final result (*bottom*). Warping of the anatomy of patient INSERM #1 is presented as a *white surface*. Original binary segmentation is presented in as a *red surface* (color figure online)

patient KCL #24 spans along the whole wall. The abnormality peak at end diastole (78 and 82 % of cardiac cycle) corresponds to late ventricular filling.

3.5.2 Response

Considering the information in Table 1, and based on volume response, patients #16 and #24 were clear responders to CRT. On the other hand, patients #12 and #9 were non-responders. This correlates well with our observations from the abnormality maps.

4 Can in silico electromechanical simulations improve our understanding of intra-ventricular mechanical dyssynchrony?

As was described in the previous section, the mechanics of dyssynchrony of CRT candidates can differ greatly from patient to patient. As a result, to be able to apply electromechanical simulations to CRT planning, we must personalize our computer models as much as possible. To obtain a *personalized* simulation, the models should include parameters that can either be measured or inferred from clinical data. Other parameters are measurements obtained from animal or ex-vivo studies. The integration of these multiple sources is therefore not a trivial task. We describe next our advances towards personalized electromechanical simulations of cardiac function in CRT candidates.

4.1 Modeling the anatomy

In order to build a computer model that can accurately represent each patient's heart, we follow several steps.

4.1.1 Segmentation

We require a biventricular anatomy to be able to include the contribution of the right ventricle (RV) to the septal wall. Thus, we extract this anatomy from MRI datasets using the segmentation algorithm implemented in [45]. In this manner, we can select the most appropriate cardiac frame as geometrical reference for the simulations. This technique is based on a deformable model that can be deformed manually, if final corrections are needed. Due to the image resolution of MRI datasets, segmenting the RV is particularly challenging. We cope with this by segmenting only the RV endocardium. As a post-processing, we add the RV epicardium with a user defined wall thickness (typically 4 mm). From this biventricular surface we generate a volumetric binary image (see Fig. 6).

4.1.2 Volumetric meshing

From the binary image we extract a polygonal surface using the Marching cubes algorithm [28]. Then, we use ReMesh [3] to smooth and ensure a manifold triangular mesh. During the volumetric meshing process, we can generate different configurations targeted to the desired simulation: high-resolution tetrahedral meshes for detailed electrophysiological

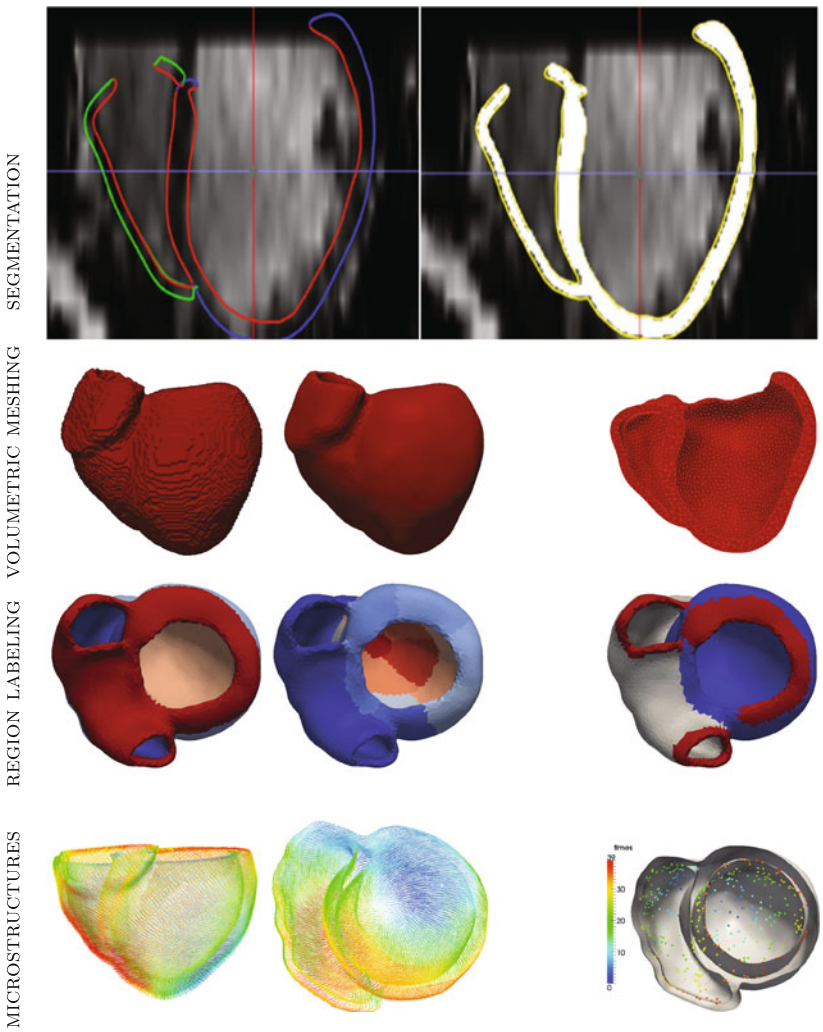

Fig. 6 Modeling the anatomy of patient INSERM #1 (from *top* to *bottom*): extracting geometry from MR datasets, generating volumetric meshes, adding labels of anatomical regions and including microstructures

simulations, low-resolution tetrahedral meshes for fast electromechanical simulations, and, high-order hexahedral meshes for mechanical simulations. For the generation of tetrahedral meshes, we use Tetgen[2] and Netgen.[3] However, the generation of patient-specific high-order hexahedral meshes is more challenging. We developed a method to build high-order meshes from a binary segmentation (see Fig. 5) [25]. These meshes allow us to perform mechanical simulations with solvers such as OpenCMISS [6].

4.1.3 Region labeling

During this step, each tetrahedron is automatically labeled according to certain anatomical regions. The labels were already defined in the original deformable model used for segmentation. Therefore, we can simply transfer the labels to the closest element in the new volumetric mesh. The regions previously defined were: valves, LV myocardium, RV myocardium, LV surface, RV surface, epicardial surface and the 17 myocardial AHA segments (Fig. 6). Some labels will be used for mechanical and electrophysiological simulation personalization. Other labels will be used for microstructures inclusion.

4.1.4 Microstructures inclusion

Some anatomical features, although very relevant for generating realistic simulations, cannot be retrieved in vivo with current imaging techniques. Therefore, we include them in our anatomical model based on ex vivo observations. The two main structures we require for simulation are preferential myocardial fiber orientation (myofibers) and the cardiac conduction system (Purkinje networks). Further details will be provided in the next section.

4.2 Modeling the electrophysiology

Classic electrophysiological (EP) models include ionic models that characterize ionic currents flowing through the

[2] http://tetgen.berlios.de.

[3] http://www.hpfem.jku.at/netgen.

cardiac cell membrane [9]. This type of models use many parameters to recreate in detail events that happen at the cellular level. Unfortunately, due to high computational cost, that will limit its use in clinical environment, detailed EP models are not directly translatable to our CRT application. To cope with this constraint, we have developed simple phenomenological models of electrophysiology, as described in [35]. The method uses the Eikonal form of the Hamilton–Jacobi equation to model electrophysiological wave propagation in the myocardium. Anisotropic conduction due to the myofibers structure is included in the domain considering the myocyte direction distribution calculated by means of the Streeter model [42]. A fast marching method (FMM) is applied to the numerical solution in the domain for myocardium. We use homogeneous conduction velocities of 0.67 and 0.235 m/s along myofibers direction and transverse to myofibers direction, respectively [35]. In order to include the effect of the cardiac conduction system, we defined a virtual Purkinje partial-mesh that started in the apex of both ventricles and is deployed throughout the ventricles. Following observations reported by Durrer et al. [21], we bounded the activation time of the Purkinje terminals to a maximum of 40 ms from the first terminal activated in the apex to the last one in the base [7]. Purkinje terminal distribution was generated randomly and gave a total of 300 points in the LV and 150 in the RV (Fig. 6).

One common electrical disorder among CRT candidates is left bundle branch block (LBBB). This disorder has been widely associated with intra-ventricular dyssynchrony [34]. The close link between LBBB (electrical defect) and intra-ventricular dyssynchrony (mechanical defect) has been studied in animal models [43], clinical subjects [19], and, more recently in computational models [24]. However, the respective influence of one defect on the other remains an open issue.

To model LBBB, we consider first the activation of the Purkinje system in the RV, and the retrograde activation of the Purkinje system in the LV after the depolarization wave crossed the septal wall and reached the first LV Purkinje terminal (Fig. 7). Besides simulating LBBB, we personalize the EP model further by including local activation time information measured with EnSite as described in [37]. Briefly, we use a fast Eikonal model to make an initial tissue conductivity estimation. We use an adaptive multi-level domain decomposition algorithm to minimize the mean-squared difference of the simulated and measured isochrones. Then we set this estimate as the conductivity parameter of a biophysical model (Mitchell–Schaeffer). Additional parameters, related to action potential duration

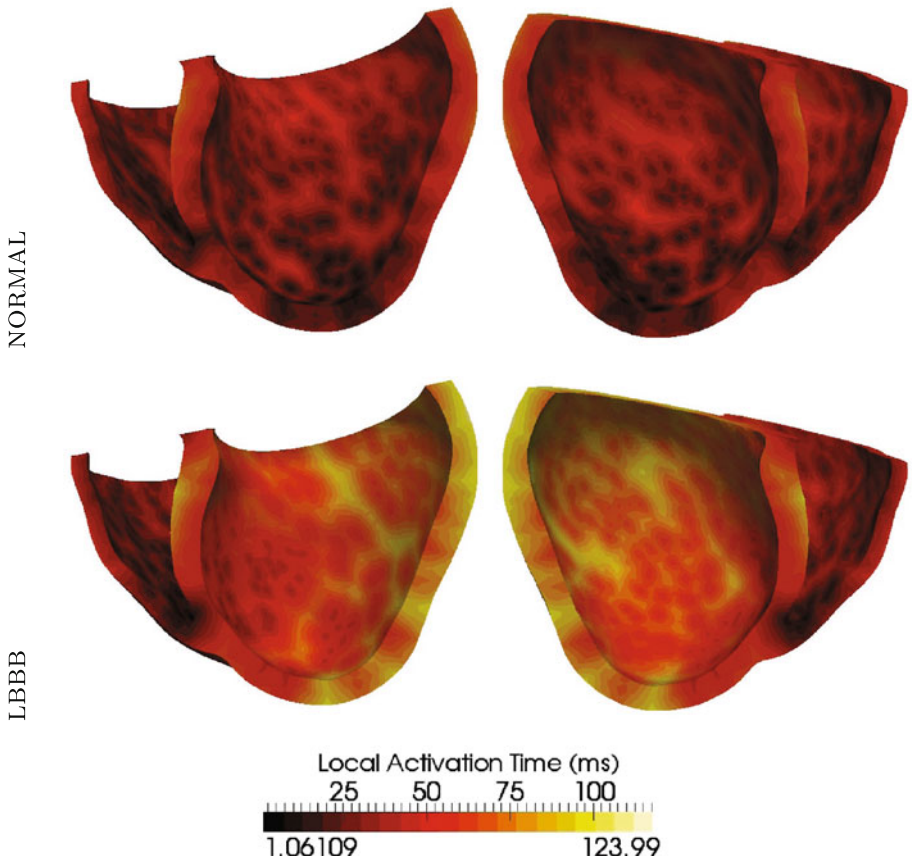

Fig. 7 Electrophysiological simulation for a normal activation pattern (*top*) and for a left bundle branch block activation pattern (LBBB) (*bottom*). Isochrone map of local activation time in ms

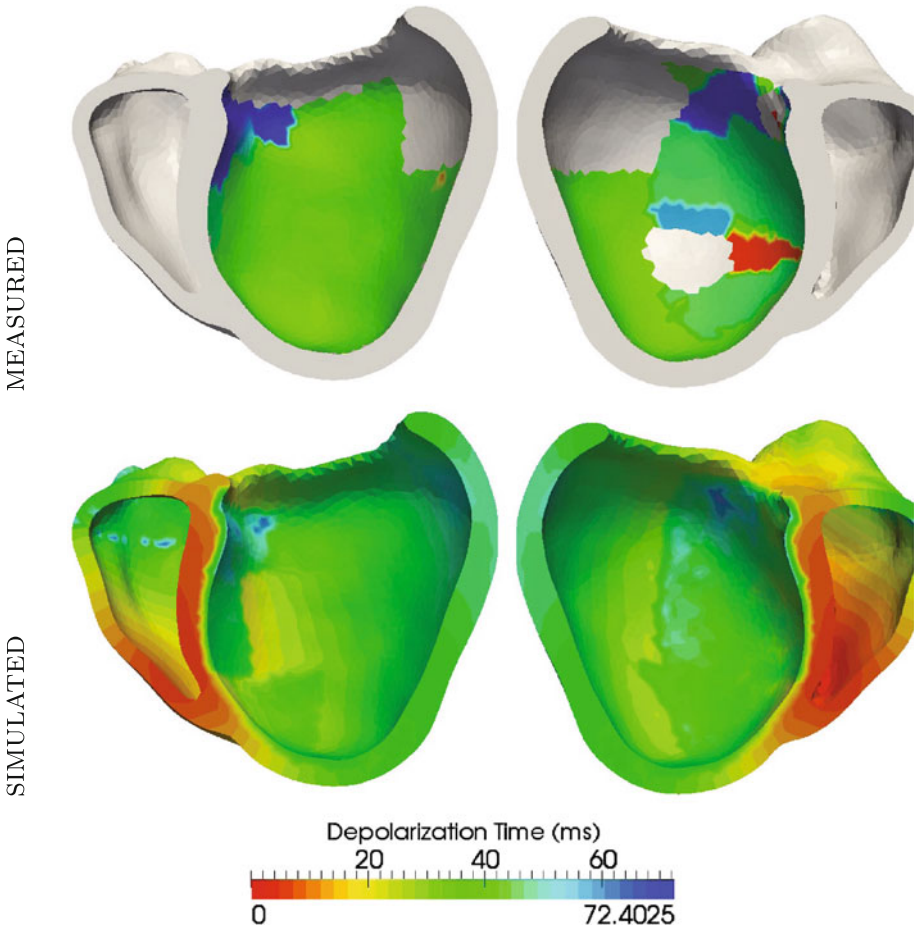

Fig. 8 Personalized electrophysiological simulation. Depolarization time (DT) isochrones as measured with EnSite in the left ventricle (*top*). Including the measured DTs into the EP simulation, we obtain DT isochrones on the whole biventricular anatomy (*bottom*)

and restitution properties of the tissue, are then directly estimated locally using the Mitchell–Schaeffer model and the measured endocardial surface potential. With this approach, the simulated activation patterns are optimized to fit the measured activation patterns. The obtained EP model is displayed in Fig. 8.

4.3 Modeling the mechanics

With the steps described in Sects. 4.1 and 4.2, we accomplished geometrical and electrophysiological personalization. For mechanical personalization, we performed an automatic calibration of the parameters based on global physiological indicators and cardiac motion specific to the patient as follows. The fast EP models were integrated into the finite element mechanical framework SOFA [1]. The simulation presented in this study was obtained with an updated implementation of the Bestel–Clement–Sorine model described in [40]. To prevent rigid body motion, some approaches choose to impose fixed zero Dirichlet boundary conditions at the apex (or even the base). In our case, to better resemble physiological conditions, we used two types of boundary conditions. First, the volumetric mesh was attached to soft springs at the level of the four valve annuli limiting ventricular global motion. To allow some valve motion, these linear springs were connected to the valve vertices at their reference position (stiffness = 50 Pa). The same spring approach was used to constrain the apex. Second, we defined a fixed pericardium surface surrounding the myocardium (fixed distance of 2 mm from the epicardium). A contact force allows sliding of the myocardium against the pericardium. Both pericardium and apex constraints limited ventricular displacements [30].

The cardiac motion was computed from cine SSFP datasets using the TDFFD registration algorithm (see Sect. 3.2). The static volumetric mesh (Sect. 4.1) was deformed using the transformation obtained from the registration. With this deformed volumetric mesh, the patient's volume curve was computed. Next, the ventricular pressure was computed using as boundary condition a Windkessel model that depends on four parameters: the peripheral resistance, the characteristic time, the characteristic resistance and the total arterial inertia [40]. With this volume and pressure information, we implemented a new method to calibrate the hyperelastic constitutive parameters and the Windkessel parameters required for the mechanical simulation. This calibration method was proposed to tackle two issues: the

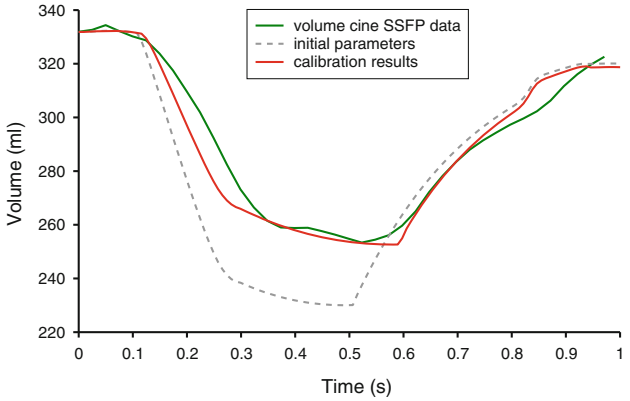

Fig. 9 Results of the automatic calibration of mechanical simulation parameters for patient INSERM #1. The optimization uses the ventricular volume curve computed from image data

choice of the parameters to estimate and their initial calibration to ensure convergence. The method automatically calibrates the parameters from the ventricular volume curve computed from image data (see Fig. 9).

This approach was designed to ensure speed and automatic convergence, which is highly desirable for our clinical application. Although a clear simplification of the cardiac events happening during cardiac contraction, this method proved to correctly reproduce ventricular volume/pressure relationships both in volunteers and in heart failure patients [31]. The calibration can be further enriched with personalization based on local volumes (i.e., per AHA segment) or on motion information (i.e., position of the endocardial surfaces).

The method is based on the unscented transform algorithm and requires only one iteration with multiple simulations performed in parallel for calibrating typically 4 or 5 parameters selected from a sensitivity analysis. The parameters evaluated included active contractive components (i.e., contraction, stiffness, relaxation rate, viscosity), passive hyperelastic components (i.e., Mooney Rivlin material), and hemodynamics components (i.e., Windkessel model). This algorithm builds a covariance matrix between the relevant parameters and the observations (in our case the minimum of the LV volume and the minimum and the maximum of its derivative) spread around an initial parameter set. The new parameters are then found to minimize the difference between the mean simulated observations and the measured observations in one iteration. Complete details can be found in [30].

4.4 Resulting electromechanical simulations

Figure 10 shows the electromechanical simulations obtained for the four cases from INSERM. In general, RV motion was well reproduced, compared to the contours obtained from cine SSFP datasets, except towards the ES phase at the basal level. For the LV, the motion of the anterior, lateral and posterior walls were well reproduced. As for the septum, the simulations generated an early motion, probably due to an early activation of the septum resulting from an unbalanced contribution of the RV. However, this motion is not synchronized with the septal motion observed in the patients. The lack of electrical information from the RV endocardium does not allow to properly personalize the electrical model. Evidently, modeling the mechanic interactions leading to septal flash remains a challenge. This might require a better parameterization of the current model in order to obtain more accurate results. Improvements can be related to an extended hemodynamic model and/or personalization of additional parameters. This is further discussed in Sects. 5.3 and 6.

5 Discussion

5.1 CRT candidate selection

One major point to take into account is the lack of standardization of *response criteria*. As recently pointed out by Fornwalt: "Methods to assess response to CRT are nearly as varied and different as the numerous published dyssynchrony parameters" [23]. Specifically, clinical response evaluates whether the patient *feels better*, which depends on many factors besides the therapy itself. Volume response evaluates whether the heart *works better*, but this in turn may be affected by artifacts in pre-/post-CRT images. These criteria partially reflect hemodynamic changes resulting from CRT. They do not consider improvements in the contraction or synchronization of the ventricular walls, which would be the first improvement of cardiac function to be expected from CRT. This was one of the main motivations to develop a technique for abnormal motion quantification [18]. Another strong limitation is that the definitions of both clinical and volume responses include arbitrary thresholds that the patient should pass to be considered a responder. This limitation was partially addressed by Foley et al. [22] by suggesting an evaluation based on a spectrum of responses. Note that the literature on CRT studies also makes a distinction between ischemic and non-ischemic patients, and reports different rates of response for both categories. However, and contrary to our study, few works actually target the characterization of specific patterns of dyssynchrony and their possible relation with the scar location.

Applying this spectrum of responses concept, we may categorize our population into several groups. (1) Pure LBBB with septal flash.[4] These patients tend to respond

[4] Early inward motion/contraction of the septum, followed by lateral wall contraction. This latter contraction pulls the relaxed septum and thereby *stretches* it (see animations in supplementary material).

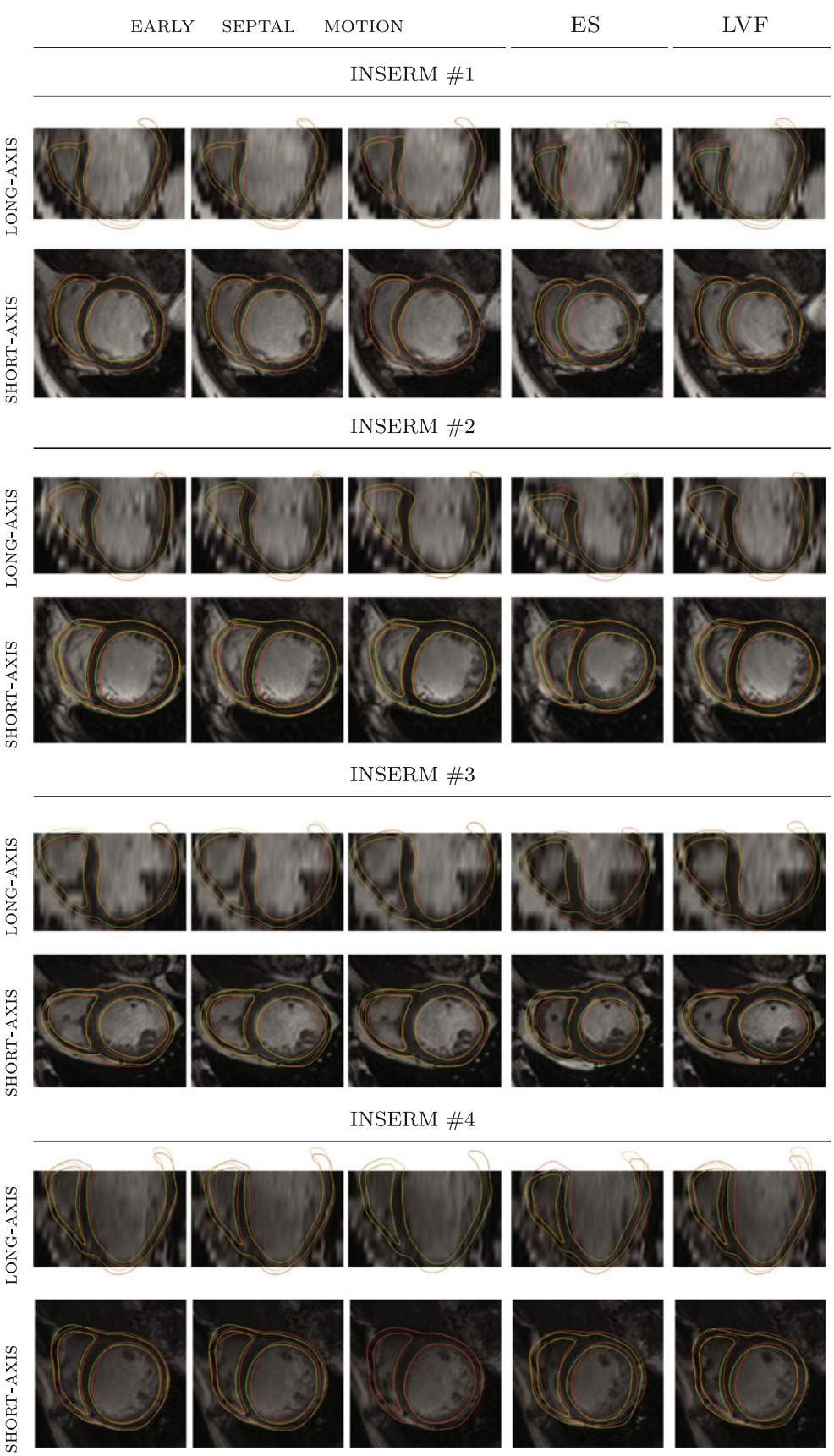

Fig. 10 To personalize the electromechanical simulation, we extract cardiac motion information from cine SSFP data using image registration [14]. A patient-specific volume curve is obtained from the deformed mesh (*green*). The mechanical simulation is optimized to fit this patient-specific volume curve (*red*). *ES* end systole, *LVF* late ventricular filling. See animations in supplementary material (color figure online)

positively to CRT. From our population, patients INSERM #1, INSERM #4 and KCL #24 correspond to this category and were responders. (2) LBBB with septal scar. These patients tend to respond poorly to CRT [20]. In our population, KCL #12 and KCL #9 fall into this category and were non-responders. (3) LBBB with non-septal scar. As long as the leads can be placed in viable tissue, patients with inferior/lateral scar have slightly higher response rate [20]. In our population, KCL #16 falls into this category and was a responder.

A remarkable example from our population is INSERM #2 who showed abnormal septal motion, but in smaller magnitude and responded positively to the therapy. This confirms the presence of additional mechanisms involved in CRT that require further investigation.

5.2 Computational models to understand mechanical dyssynchrony

The cardiovascular system has been studied for decades using in vitro and animal models. More recently, computational models have also been adopted as a technique able to accurately reproduce cardiovascular dynamics.

Using a generic (non-personalized) simulation, the study of Leenders et al. [27] helped us understand different patterns of dyssynchrony. They investigated intra-ventricular mechanical dyssynchrony by analyzing septal deformation patterns. In this study, 132 CRT candidates with LBBB were categorized in 3 septal deformation patterns. They used a simplified lumped model (0D) to simulate beat-by-beat hemodynamics [2, 29]. Although this model is not personalized, it proved to be very helpful for understanding the mechanics behind SF. This model (TriSeg) represents the geometry with three ellipsoids corresponding to RV, septum and LV. Simulations included different activation delays between the septal and lateral wall, together with different severities of hypo-contractility. The three types of septal deformation patterns were reproduced by simulating: (1) pure LBBB, (2) LBBB with decreased septal contractility, and (3) LBBB with decreased global contractility (e.g., severely infarcted heart). The study showed that response to CRT was higher in pattern 1 and decreased towards pattern 3. These observations actually confirm the general trend observed in our images and expectations towards the location and presence of an infarcted area, as discussed in Sect. 5.1.

In another recent electromechanical simulation study, Kerckhoffs et al. [24] used a canine heart model to investigate the development of intra-ventricular dyssynchrony. The study showed that mechanical dyssynchrony arises from the combination of electrical dyssynchrony, increase in total blood volume, and ongoing dilatation.

5.3 Computational models to simulate the effect of CRT

The location of the pacing leads has been shown to greatly influence the success of CRT [11]. Thus, predicting optimal pacing sites is the ultimate purpose of our patient-specific electromechanical simulations. Several approaches have been explored to personalize the electromechanical models.

Sermesant et al. [40] reported preliminary results on the patient-specific electromechanical simulation methodology presented in the current study. We extended the methodology to include kinematic information (i.e., cardiac motion from cine SSFP) and the automatic calibration of mechanical parameters [30].

Recent studies have explored the use of detailed electromechanical simulations to study the effect of CRT. Constantino et al. [10] used a non-personalized detailed electromechanical model on a patient-specific anatomy to study the activation sequence in normal and failing hearts. Niederer et al. [33] used detailed electromechanical simulations to locate optimal pacing sites using invasive data from a 60-year-old female. The study included a personalized anatomy with a generic (non-personalized) posterolateral scar and took into account manually aligned coronary venous anatomy from the same patient.

A very important aspect to consider is that the simulations should reproduce the long-term effects of the therapy. Kerckhoffs et al. [24] suggested to combine growth models with electromechanical simulations. These growth models are based on physiological processes such as hypertrophy and/or dilation due to pressure and/or volume overload. By including these growth models and more detailed boundary conditions (CircAdapt [2]), Kerckhoffs et al. [24] were able to reproduce the SF events with a finite-element canine model. Further extension to patient-specific applications is required.

5.4 An integrated pipeline for personalization

With our pipeline, we managed to enrich the clinical data available for the personalization of computational models. We could achieve it by extending routine imaging data with advanced imaging data. In particular, we have collected experimental MRI sequences, including 3DTAG [39], whole-heart [46], and 3D MR angiography sequences. We have developed techniques to extract valuable anatomical and functional information from these sequences, as reported in previous publications: myocardial deformation from 3DTAG [15], full heart anatomy [36] and coronary tree [48]. Both chamber and coronary information are spatially fused and can be visualized during CRT interventions using an X-ray/MR (XMR) hybrid imaging

system [38]. Our pipeline is integrated into a common software framework (i.e., CRT planning platform). The CRT planning platform allows for a more efficient case processing workflow, with respect to multiple pieces of unconnected software.

6 Conclusions and future work

To understand and improve CRT, we investigated two aspects in this study: pre-operative multimodal image data and patient-specific computational models. From our observations, along with the studies discussed above (Sect. 5), we can conclude the following.

First, image-based criteria can complement the current criteria for selecting CRT candidates. Nonetheless, special care is required for preserving the quantitative information embedded in such mechanical dyssynchrony indices, and not reducing them to the definition of yet another threshold for CRT patient selection. Rather, the likelihood of response should be analyzed based on a deeper understanding of the dyssynchrony patterns of each given patient and the chances of properly delivering the therapy given the patient substrate. By analyzing pre-operative multimodal image data, we can identify the dyssynchrony patterns that will most likely benefit from CRT. In addition, computational models can help to discriminate between non-responders originated from a lack of electrical resynchronization, problems of tissue stimulation (e.g., large scar areas), or mechanical defects.

Second, modeling the electrical defect (LBBB) alone is not enough to capture the mechanisms of intra-ventricular dyssynchrony. From the insights obtained from our pre-operative image data, we observed that dyssynchrony mechanisms can vary significantly among CRT candidates. Thus, there is a need for electromechanical simulations that accurately reproduce patient-specific dyssynchrony patterns.

Third, several recent studies suggest the strong potential of electromechanical models to reproduce the effect of CRT on patients. In our study, we observed that with a correct personalization of the eletrophysiological model, abnormal septal motion is retrievable. However, we believe that the whole phenomenon of septal flash, including interventricular pressure differences, lateral pulling and septal stretching, requires further investigation. For instance, parametrization of current electromechanical models should be improved through better electromechanical coupling, inclusion of patient-specific viability information (i.e., scar) and plausible anatomical locations of pacing (i.e., coronary tree), more detailed boundary conditions (e.g., hemodynamics computed by the CircAdapt model), and inclusion of growth models to evaluate the chronic effect of the therapy. Once these issues are tackled, we can further explore the potential of patient-specific electromechanical models to assess whether synchronicity is restored after an in silico CRT device implantation.

Fourth, in this study we present a large amount of multimodal imaging data from CRT candidates. To our knowledge, such an amount of complementary image data had never been used to study CRT candidates, due to the difficulty of acquiring these datasets. This information proved to be highly valuable to understand the complexity of the mechanisms conditioning CRT response. Now that we have a pipeline in place, it is possible to increase the sample size and evaluate multiple pacing sites. Our future work will focus on the evaluation of a larger cohort of patients recruited within the euHeart project. With this we hope to make electromechanical simulations ready to be applied in real clinical scenarios.

Acknowledgments This work was partially funded by the Spanish Ministry of Innovation and Science (CEN-20091044, TIN2009-14536-C02-01 and TIN2011-28067), and the European Commission Seventh Framework Programme (FP7-ICT-2007-2-224495).

References

1. Allard J, Cotin S, Faure F, Bensoussan PJ, Poyer F, Duriez C, Delingette H, Grisoni L (2007) Sofa an open source framework for medical simulation. In: Medicine meets virtual reality (MMVR'15). Long Beach, USA
2. Arts T, Delhaas T, Bovendeerd P, Verbeek X, Prinzen FW (2005) Adaptation to mechanical load determines shape and properties of heart and circulation: the CircAdapt model. Am J Physiol Heart Circ Physiol 288(4):H1943–H1954
3. Attene M, Falcidieno B (2006) ReMESH: an interactive environment to edit and repair triangle meshes. In: IEEE international conference on shape modeling and applications, p 41
4. Auricchio A, Prinzen FW (2011) Non-responders to cardiac resynchronization therapy: the magnitude of the problem and the issues. Circ J 75(3):521–527
5. Bleeker GB, Bax JJ, Fung JWH, van der Wall EE, Zhang Q, Schalij MJ, Chan JYS, Yu CM (2006) Clinical versus echocardiographic parameters to assess response to cardiac resynchronization therapy. Am J Cardiol 97(2):260–263
6. Bradley C, Bowery A, Britten R, Budelmann V, Camara O, Christie R, Cookson A, Frangi AF, Gamage TB, Heidlauf T, Krittian S, Ladd D, Little C, Mithraratne K, Nash M, Nickerson D, Nielsen P, Nordbø O, Omholt S, Pashaei A, Paterson D, Rajagopal V, Reeve A, Röhrle O, Safaei S, Sebastián R, Steghöfer M, Wu T, Yu T, Zhang H, Hunter P (2011) OpenCMISS: a multi-physics and multi-scale computational infrastructure for the VPH/Physiome project. Prog Biophys Mol Biol 107(1):32–47
7. Camara O, Sermesant M, Lamata P, Wang L, Pop M, Relan J, De Craene M, Delingette H, Liu H, Niederer S, Pashaei A, Plank G, Romero D, Sebastian R, Wong KCL, Zhang H, Ayache N, Frangi AF, Shi P, Smith NP, Wright GA (2011) Inter-model consistency and complementarity: learning from ex-vivo imaging and electrophysiological data towards an integrated understanding of cardiac physiology. Prog Biophys Mol Biol 107(1):122–133
8. Casanova C, Celli BR, Barria P, Casas A, Cote C, de Torres JP, Jardim J, Lopez MV, Marin JM, de Oca MM, Pinto-Plata V,

Aguirre-Jaime A (2011) The 6-min walk distance in healthy subjects: reference standards from seven countries. Eur Respir J 37(1):150–156
9. Clayton RH, Bernus O, Cherry EM, Dierckx H, Fenton FH, Mirabella L, Panfilov AV, Sachse FB, Seemann G, Zhang H (2011) Models of cardiac tissue electrophysiology: progress, challenges and open questions. Prog Biophys Mol Biol 104(1–3):22–48
10. Constantino J, Hu Y, Trayanova NA (2012) A computational approach to understanding the cardiac electromechanical activation sequence in the normal and failing heart, with translation to the clinical practice of CRT. Prog Biophys Mol Biol 110(2–3): 372–379
11. Cowburn PJ, Leclercq C (2012) How to improve outcomes with cardiac resynchronisation therapy: importance of lead positioning. Heart Fail Rev 17(6):781–9
12. De Craene M, Duchateau N, Tobon-Gomez C, Ghafaryasl B, Piella G, Rhode K, Frangi AF (2012) Spm to the heart: mapping of 4D continuous velocities for motion abnormality quantification. In: 2012 IEEE International symposium on biomedical imaging: from nano to macro
13. De Craene M, Piella G (2012) An implementation of TDFFD and LDFFD algorithms. Insight J 63
14. De Craene M, Piella G, Camara O, Duchateau N, Silva E, Doltra A, D'hooge J, Brugada J, Sitges M, Frangi AF (2012) Temporal diffeomorphic free-form deformation: application to motion and strain estimation from 3D echocardiography. Med Image Anal 16(2):427–450
15. De Craene M, Tobon-Gomez C, Butakoff C, Duchateau N, Piella G, Rhode KS, Frangi AF (2012) Temporal diffeomorphic free form deformation (TDFFD) applied to motion and deformation quantification of tagged MRI sequences. In: Camara O, Konukoglu E, Pop M, Rhode K, Sermesant M, Young A (eds) Statistical atlases and computational models of the heart. Imaging and modelling challenges. Lecture Notes in Computer Science, vol 7085, Springer Berlin, pp 68–77
16. Duchateau N, Craene MD, Piella G, Frangi AF (2012) Constrained manifold learning for the characterization of pathological deviations from normality. Med Image Anal 16(8):1532–1549
17. Duchateau N, De Craene M, Piella G, Silva E, Doltra A, Sitges M, Bijnens BH, Frangi AF (2011) A spatiotemporal statistical atlas of motion for the quantification of abnormal myocardial tissue velocities. Med Image Anal 15(3):316–328
18. Duchateau N, Doltra A, Silva E, De Craene M, Piella G, Castel MA, Mont L, Brugada J, Frangi AF, Sitges M (2012) Atlas-based quantification of myocardial motion abnormalities: added-value for understanding the effect of cardiac resynchronization therapy. Ultrasound Med Biol 38(12):2186–2197
19. Duckett SG, Camara O, Ginks MR, Bostock J, Chinchapatnam P, Sermesant M, Pashaei A, Lambiase PD, Gill JS, Carr-White GS, Frangi AF, Razavi R, Bijnens BH, Rinaldi CA (2012) Relationship between endocardial activation sequences defined by high-density mapping to early septal contraction (septal flash) in patients with left bundle branch block undergoing cardiac resynchronization therapy. Europace 14(1):99–106
20. Duckett SG, Ginks M, Shetty A, Kirubakaran S, Bostock J, Kapetanakis S, Gill J, Carr-White G, Razavi R, Rinaldi CA (2012) Adverse response to cardiac resynchronisation therapy in patients with septal scar on cardiac MRI preventing a septal right ventricular lead position. J Interv Card Electrophysiol 33(2):151–160
21. Durrer D, van Dam RT, Freud GE, Janse MJ, Meijler FL, Arzbaecher RC (1970) Total excitation of the isolated human heart. Circulation 41(6):899–912
22. Foley PWX, Leyva F, Frenneaux MP (2009) What is treatment success in cardiac resynchronization therapy?. Europace 11(Suppl 5):v58–v65
23. Fornwalt BK (2011) The dyssynchrony in predicting response to cardiac resynchronization therapy: a call for change. J Am Soc Echocardiogr 24(2):180–184
24. Kerckhoffs RC, Omens JH, McCulloch AD (2012) Mechanical discoordination increases continuously after the onset of left bundle branch block despite constant electrical dyssynchrony in a computational model of cardiac electromechanics and growth. Europace 14(Suppl 5):v65–v72
25. Lamata P, Niederer S, Nordsletten D, Barber DC, Roy I, Hose DR, Smith N (2011) An accurate, fast and robust method to generate patient-specific cubic hermite meshes. Med Image Anal 15(6):801–813
26. Larrabide I, Omedas P, Martelli Y, Planes X, Nieber M, Moya J, Butakoff C, Sebastián R, Camara O, De Craene M, Bijnens B, Frangi A (2009) GIMIAS: an open source framework for efficient development of research tools and clinical prototypes. In: Ayache N, Delingette H, Sermesant M (eds) Functional imaging and modeling of the heart. Lecture Notes in Computer Science, vol 5528, Springer Berlin, pp 417–426
27. Leenders GE, Lumens J, Cramer MJ, Boeck BWLD, Doevendans PA, Delhaas T, Prinzen FW (2012) Septal deformation patterns delineate mechanical dyssynchrony and regional differences in contractility: analysis of patient data using a computer model. Circ Heart Fail 5(1):87–96
28. Lorensen WE, Cline HE (1987) Marching cubes: a high resolution 3D surface construction algorithm. Comput Graph 21(4):163–169
29. Lumens J, Delhaas T, Kirn B, Arts T (2009) Three-wall segment (triseg) model describing mechanics and hemodynamics of ventricular interaction. Ann Biomed Eng 37(11):2234–2255
30. Marchesseau S, Delingette H, Sermesant M, Ayache N (2012) Fast parameter calibration of a cardiac electromechanical model from medical images based on the unscented transform. Biomech Model Mechanobiol [Epub ahead of print]
31. Marchesseau S, Delingette H, Sermesant M, Sorine M, Rhode K, Duckett S, Rinaldi C, Razavi R, Ayache N (2012) Preliminary specificity study of the Bestel–Clement–Sorine electromechanical model of the heart using parameter calibration from medical images. J Mech Behav Biomed (in press)
32. McMurray JJ, Adamopoulos S, Anker SD, Auricchio A, Böhm M, Dickstein K, Falk V, Filippatos G, Fonseca C, Gomez-Sanchez MA, Jaarsma T, Køber L, Lip GY, Maggioni AP, Parkhomenko A, Pieske BM, Popescu BA, Rønnevik PK, Rutten FH, Schwitter J, Seferovic P, Stepinska J, Trindade PT, Voors AA, Zannad F, Zeiher A (2012) ESC guidelines for the diagnosis and treatment of acute and chronic heart failure 2012: the task force for the diagnosis and treatment of acute and chronic heart failure 2012 of the European Society of Cardiology developed in collaboration with the Heart Failure Association (HFA) of the ESC. Eur Heart J 33(14):1787–1847
33. Niederer SA, Shetty AK, Plank G, Bostock J, Razavi R, Smith NP, Rinaldi CA (2012) Biophysical modeling to simulate the response to multisite left ventricular stimulation using a quadripolar pacing lead. Pacing Clin Electrophysiol 35(2):204–214
34. Parsai C, Bijnens B, Sutherland GR, Baltabaeva A, Claus P, Marciniak M, Paul V, Scheffer M, Donal E, Derumeaux G, Anderson L (2009) Toward understanding response to cardiac resynchronization therapy: left ventricular dyssynchrony is only one of multiple mechanisms. Eur Heart J 30(8):940–949
35. Pashaei A, Romero D, Sebastian R, Camara O, Frangi A (2011) Fast multiscale modeling of cardiac electrophysiology including purkinje system. IEEE Trans Biomed Eng 58(10):2956–2960
36. Peters J, Ecabert O, Meyer C, Kneser R, Weese J (2010) Optimizing boundary detection via simulated search with applications to multi-modal heart segmentation. Med Image Anal 14(1):70–84
37. Relan J, Chinchapatnam P, Sermesant M, Rhode K, Ginks M, Delingette H, Rinaldi CA, Razavi R, Ayache N (2011) Coupled

personalization of cardiac electrophysiology models for prediction of ischaemic ventricular tachycardia. J R Soc Interface 1(3): 396–407
38. Rhode KS, Sermesant M, Brogan D, Hegde S, Hipwell J, Lambiase P, Rosenthal E, Bucknall C, Qureshi SA, Gill JS, Razavi R, Hill DLG (2005) A system for real-time XMR guided cardiovascular intervention. IEEE Trans Med Imaging 24(11): 1428–1440
39. Rutz AK, Ryf S, Plein S, Boesiger P, Kozerke S (2008) Accelerated whole-heart 3D CSPAMM for myocardial motion quantification. Magn Reson Med 59(4):755–763
40. Sermesant M, Chabiniok R, Chinchapatnam P, Mansi T, Billet F, Moireau P, Peyrat JM, Wong K, Relan J, Rhode K, Ginks M, Lambiase P, Delingette H, Sorine M, Rinaldi CA, Chapelle D, Razavi R, Ayache N (2012) Patient-specific electromechanical models of the heart for the prediction of pacing acute effects in CRT: a preliminary clinical validation. Med Image Anal 16(1):201–215
41. Smith N, de Vecchi A, McCormick M, Nordsletten D, Camara O, Frangi AF, Delingette H, Sermesant M, Relan J, Ayache N, Krueger MW, Schulze WHW, Hose R, Valverde I, Beerbaum P, Staicu C, Siebes M, Spaan J, Hunter P, Weese J, Lehmann H, Chapelle D, Rezavi R (2011) euHeart: personalized and integrated cardiac care using patient-specific cardiovascular modelling. Interface Focus 1(3):349–364
42. Streeter DD, Spotnitz HM, Patel DP, Ross J, Sonnenblick EH (1969) Fiber orientation in the canine left ventricle during diastole and systole. Circ Res 24(3):339–347
43. Strik M, van Middendorp LB, Vernooy K (2012) Animal models of dyssynchrony. J Cardiovasc Transl Res 5(2):135–45
44. Tobon-Gomez C, De Craene M, Dahl A, Kapetanakis S, Carr-White G, Lutz A, Rasche V, Etyngier P, Kozerke S, Schaeffter T, Riccobene C, Martelli Y, Camara O, Frangi AF, Rhode KS (2012) A multimodal database for the 1st cardiac motion analysis challenge. In: Camara O, Konukoglu E, Pop M, Rhode K, Sermesant M, Young A (eds) Statistical atlases and computational models of the heart. Imaging and modelling challenges. Lecture Notes in Computer Science, vol 7085, Springer, Berlin, pp 33–44
45. Tobon-Gomez C, Sukno FM, Butakoff C, Huguet M, Frangi AF (2012) Automatic training and reliability estimation for 3D ASM applied to cardiac MRI segmentation. Phys Med Biol 57(13): 4155
46. Uribe S, Muthurangu V, Boubertakh R, Schaeffter T, Razavi R, Hill DL, Hansen MS (2007) Whole-heart cine MRI using real-time respiratory self-gating. Magn Reson Med 57(3):606–613
47. van Deursen C, van Geldorp IE, Rademakers LM, van Hunnik A, Kuiper M, Klersy C, Auricchio A, Prinzen FW (2009) Left ventricular endocardial pacing improves resynchronization therapy in canine left bundle-branch hearts. Circ Arrhythm Electrophysiol 2(5):580–587
48. Velut J, Lentz PA, Boulmier D, Coatrieux JL, Toumoulin C (2011) Assessment of qualitative and quantitative features in coronary artery MRA. IRBM 32(4):229–242
49. Worsley KJ, Andermann M, Koulis T, MacDonald D, Evans AC (1999) Detecting changes in nonisotropic images. Hum Brain Mapp 8(2–3):98–101